Large Eddy Simulations of the turbulent flow in curved ducts: influence of the curvature radius

Cécile Münch and Olivier Métais

L.E.G.I. B.P. 53, 38041 Grenoble Cedex 09, France cecile.munch@hmg.inpg.fr

Summary. We present Large-Eddy Simulations (LES) of the turbulent compressible flow in curved ducts of square cross section. The aim is to investigate the influence of the curvature radius R_c on the flow and the heat transfer. We consider three different curvature radii : $4D_h$, $7D_h$ and $11D_h$ (D_h hydraulic diameter). We observe a rise in the number of streamwise vortices of Görtler type on the unstable concave wall when the curvature radius decreases. The main effect is a strong intensification of the secondary flows with the reduction of R_c: a rise of 100 % of the intensity between the smaller and the higher case of the curvature radius. We determine the influence of R_c on heat transfer by considering the case of convex wall heating. Due to the modification of the secondary flows, we observe an enhancement of the heat flux for the smaller value of the curvature radius, specially close to the sidewalls.

1 Introduction

The prediction of heat and mass transport processes in curved ducts is of interest for engineering applications like compressors, turbines, cooling ducts of rocket engines. Several experimental and numerical investigations have been performed to study the turbulent flow within a curved duct without any heating: [1, 2, 3, 4, 5, 6, 7]. These works have brought to light the destabilizing effect of the concave wall when the convex wall has conversely a stabilizing action. Resulting from this centrifugal instability, vortices, called Görtler vortices, appear on the concave wall. The combination of these vortices and of the pressure gradient between the concave and the convex wall leads to the development of an intense cross-stream flow. For numerical studies, the difficulty lies in the correct prediction of this cross-stream flow (called secondary flow) and of the related turbulence characteristics. When heat transfer and curved effect are combined, experiments are fewer. Johnson and Launder (1985) [8] investigate a heated square-sectioned U-bend and show that the heat transfer is enhanced on the concave wall and reduced on the convex side compared to a flat wall as found by Mayle et. al (1979) [9]. Hébrard et al. (2004) [10] and Münch and Métais (2005) [11], [12] study the combined effect of curvature

and heating in a closed duct for turbulent flow using the same numerical code as in the present study. Flows in curved duct are characterized by the Dean number defined as $D_e = R_e\sqrt{D_h/(2R_c)}$, where R_c is the curvature radius. We here perform Large Eddy Simulation (LES) in different curved square ducts with or without heating to investigate the influence of the curvature radius on the flow and the heat transfer. When the curvature radius is decreased, the main observations are a rise of the secondary flow intensity and consequently an enhancement of the heat flux on the heated convex wall.

2 Numerical Methods

The computer code used for our calculations solves the LES modified three dimensional compressible Navier Stokes equations in curved square ducts (see [13]).

The subgrid-scale model is the selective structure function model proposed by Lesieur and Métais (1996) [14]. To close the system formed by the momentum and energy equations , we use three supplementary relations. The Sutherland empirical law describes the molecular viscosity variation with temperature. The gas is considered as an ideal gas with the corresponding equation of state and the Prandtl number is equal to 0.7. The system of equations in generalized coordinates is solved by means of the corrector-predictor McCormack scheme with a compact extension devised by Kennedy and Carpenter (1997) [15]. The scheme is second order in time and fourth order in space.

One original feature of the present computation is that a fully developed turbulent state is achieved at the duct inlet. To provide this fully turbulent inlet boundary condition in the curved duct, a LES of a longitudinally periodic duct of sufficient length, with all its walls at an imposed temperature T_w, is carried out at the same time. This longitudinally straight periodic duct is linked to the spatially growing duct through the characteristics conditions proposed by Poinsot and Lele (1992) [16]. At the outflow of the curved duct, we also used these conditions by imposing the pressure. The wall boundary conditions are no-slip. The flow is characterized by a Reynolds number equal to 6000, a Mach number equal to 0.5, and the turbulent Prandtl number equal to 0.6.

We use curvilinear coordinates, s in the streamwise direction, n in the direction normal to the curved wall and z in the spanwise direction. The origin of the n coordinate is taken on the concave wall. The different lengths are normalized by the hydraulic diameter D_h. The origin O is taken at the inflow on the concave side. The geometry of the duct is represented in figure 1. We carried out simulations of three different curved ducts differing by their curvature radius R_c, the length of the straight inflow and the outflow are fixed. We consider the three cases : $R_c = 11D_h$,$7D_h$ and $4D_h$ corresponding with a Dean number equal to 1300, 1600 and 2100 respectively. The curvature angle θ is taken equal to 45 degrees in the three cases.

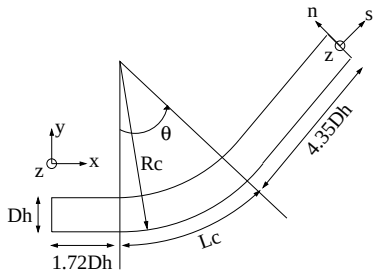

Fig. 1. Geometry of computational domain

Nonuniform numerical meshes are used with $160 * 50 * 50$, $128 * 50 * 50$ and $104 * 50 * 50$ in the s, n and z directions for $R_c = 11D_h$,$7D_h$ and $4D_h$ respectively. In the n and z directions, an hyperbolic-tangent stretching is utilized : the first node close to the wall is situated at 1.8 wall units. The reader can refer to Salinas and Métais (2002) [13] for further details.

3 Non-heated ducts

In this part, the temperature on the walls of the curved ducts is imposed to be equal to T_w. One of the appropriate ways to characterize flows in curved duct is to consider the secondary flows. In rectilinear ducts of square cross sections, a secondary transverse flow perpendicular to the bulk flow and denominated as Prandtl's second kind, appears near the duct corners. Eight counter rotating vortices, two in each corner, developed. Their intensity is relatively weak : 2% of the bulk velocity. Further downstream of the duct, curvature effects are present and new instabilities appear. The pressure gradient between the concave and the convex wall now gives rise to two intense secondary vortices called Ekman vortices [17]. We will focus our attention on this Prandtl's first kind secondary flow. In figure 2 a), we plot the maximum of the secondary flow intensity, I_{max} defined as the norm of $\mathbf{V} + \mathbf{W}$, in each cross section as a function of the streamline coordinates. We observe that the intensity grows in the three cases in the curved part and decreases progressively in the oblique outflow. The peak of the three curves is reached in the second half of the curved part. The influence of the curvature radius is clearly noticeable. I_{max} becomes higher when the curvature radius decreases, reaching more than 40 % for $R_c = 4D_h$.

To explain the growth of the intensity and dependence on the curvature radius, we have to consider the pressure coefficient, C_p, defined as $C_p = (p - p_i)/\rho U_b^2$, where p_i designates the pressure at the duct inlet. We plot the pressure coefficient in the three cases on both curved walls as a function of the streamline coordinates 2 b). In the curved part, C_p increases on the concave wall while it decreases on the convex side, as noticed by Chang

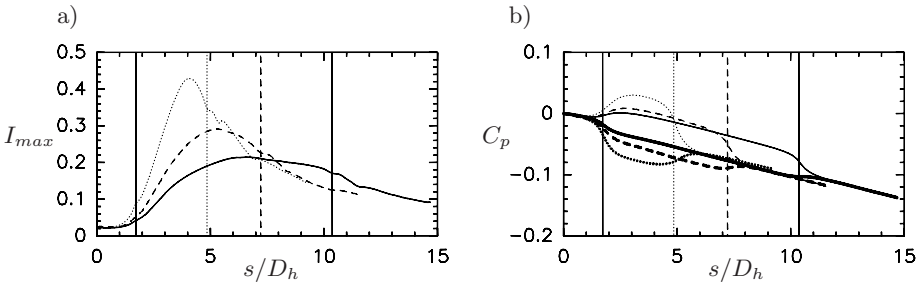

Fig. 2. a) I_{max} as a function of s, b) C_p on the concave and the **convex** walls: ——— $R_c = 11D_h$, – – – $R_c = 7D_h$, ····· $R_c = 4D_h$. The first vertical line cooresponds with the beginning of the curved part. The next three lines correspond to the end of the curved part for the three ducts.

et. al [7], Kim and Patel [4]. It creates a radial pressure gradient between the two curved wall, quasi constant, in response to the centrifugal forces. Close to the sidewalls, the velocity tends to zero whereas the pressure distribution does not vary: a secondary flow from the concave to the convex wall develops. We observe that the radial pressure gradient is stronger for the smaller value of the curvature radius: this explains the rise of a stronger secondary flow.

We now discuss the influence of this rise of intensity on the secondary flow pattern. On figure 3, we show half cross sections, taking into account the symmetry plane $z/D_h = 0.5$, of the mean secondary flow in the three cases at the duct outflow. We observe the existence of one of the Ekman

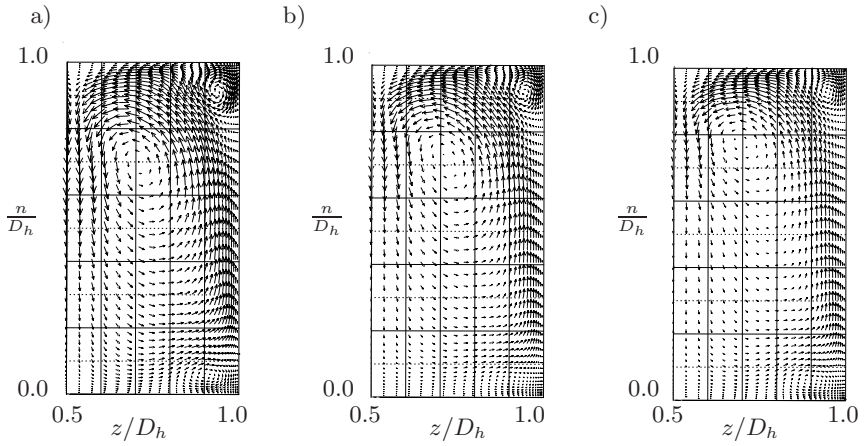

Fig. 3. Half cross sections of secondary flow at the outflow in the case a) $R_c = 4D_h$, b) $R_c = 7D_h$ and c) $R_c = 11D_h$

recirculating cells mentioned above. When R_c decreases, the center of this cell is driven toward the core region. In the case $R_c = 11D_h$, the center is indeed located at $n/D_h = 0.8$ when it is placed at $n/D_h = 0.7$ for $R_c = 4D_h$. Since the secondary flows grow in intensity, the Ekman cell is larger inducing a translation of its centre.

Another way to characterize this type of flow is to investigate the vortices. We use the Q criterion to bring out the instantaneous coherent structures in our wall shear flow, see Hunt et al. [18]. On figure 4, we show iso surfaces of positive Q with $Q = 0.7U_b^2/D_h^2$ (where U_b is the bulk velocity) in the curved part for each of the three configurations. The vortices on the concave wall are quasi longitudinal vortices originating from the straight inflow. On the concave part of the wall, they are submitted to the centrifugal instability, we observe that these coherent structures are more numerous and more intensified when the curvature radius decreases. The mean streamwise vorticity values are almost three times higher for the case $R_c = 4D_h$ than for $R_c = 11D_h$. This is attributable to the reinforcement of the centrifugal instability for smaller radii.

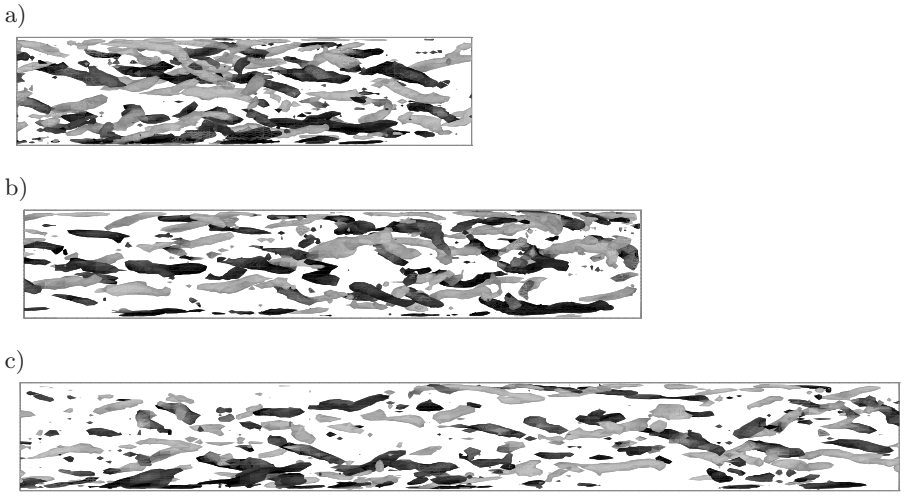

Fig. 4. Iso surfaces of $Q = 0.7$ close to the concave wall in the curved part of the case a) $R_c = 4D_h$, b) $R_c = 7D_h$ and c) $R_c = 11D_h$

4 Heated ducts

Now, we discuss the influence of the curvature radius on the heat transfer. We neglect gravitational effects and all the changes are due to compressibility. We simulate the three previous cases with a temperature on the convex wall

taken equal to twice the temperature on the three other walls. On figure 5, we represent half-cross sections of the mean secondary flow and iso values of the mean temperature at the end of the curved duct. The iso-values are plotted with a step of $0.1T_w$. We observe that the secondary flow drives hot fluid from the heated convex wall to the core region in the three cases. Closer to the sidewalls, the secondary flow bring cold fluid toward the convex wall. At this station, the intensity of the secondary flow is higher for the smaller value of R_c (cf. fig 2 a). We observe that the pocket of hot fluid develops farther from the heated wall in the normal direction when the curvature radius decreases. The ejection of hot fluid in the core region is stronger. Another aspect is the stronger transfer of cold fluid toward the heated wall for $R_c = 4D_h$. On figure 5 a), the iso values of temperature are less spaced apart in the vicinity of the convex wall, which means effectively that the temperature varies faster in this region for $R_c = 4D_h$. In the z/D_h direction, the pocket of hot fluid is larger for the larger curvature radius. The Ekman cell's center is localized closer to the sidewalls for $R_c = 11D_h$, the cold fluid remains close to the wall.

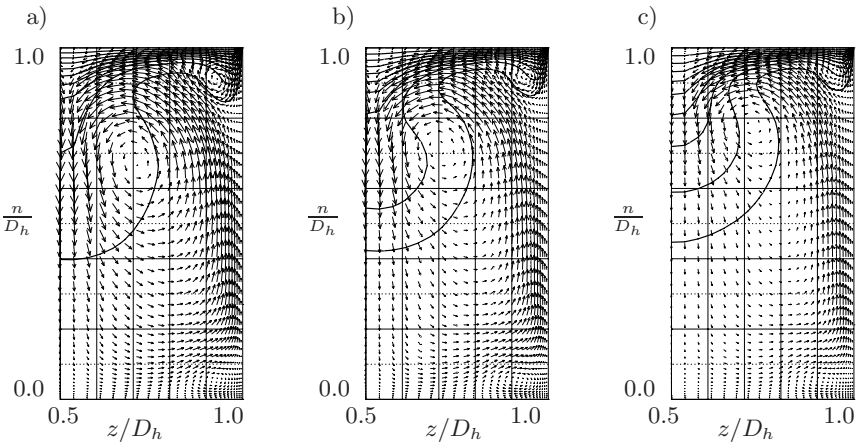

Fig. 5. Half cross sections of secondary flow and iso values of the mean temperature [step:0.1] at the outflow in the case a) $R_c = 4D_h$, b) $R_c = 7D_h$ and c) $R_c = 11D_h$

To corroborate these observations, we plot in the next figure 6, the Nusselt number on the convex heated wall as a function of the streamline coordinate and for $z/D_h = 0.5$ a) and $z/D_h = 0.25$ b). The Nusselt number is defined as:

$$Nu = H_w/(\kappa(T_w)T_w/D_h) \tag{1}$$

with H_w the wall heat flux defined as:

$$H_w = \kappa(T)\frac{\partial T(s,n,z)}{\partial n}]_{\frac{n}{D_h}=1} \tag{2}$$

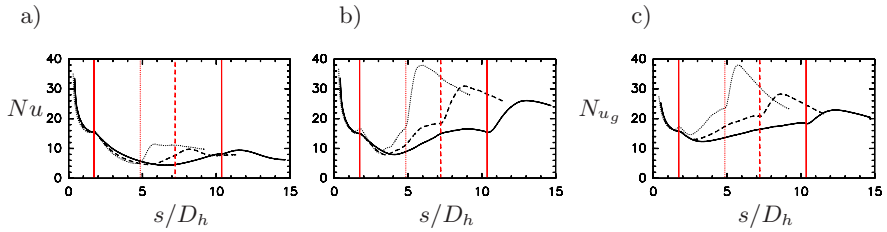

Fig. 6. Nu in the plane a) $z/D_h = 0.5$ and b)$z/D_h = 0.25$ and c) N_{u_g} as a function of s/D_h with —— $R_c = 11D_h$, – – – $R_c = 7D_h$, ····· $R_c = 4D_h$. The vertical lines correspond to beginning and the end of the curved part for the three ducts.

We also represent its mean value in the direction z/D_h, N_{u_g} on figure 6 c). For both values of z/D_h, the Nusselt number decreases in the straight inflow part due to the thermal boundary layer development. In the curved part, Nu continues to decrease for the three values of R_c in the symmetry plane. The middle plane is indeed the siege of an intense ejection of hot fluid from the heated wall associated with a weak temperature gradient and a weak heat flux. The heat flux decrease is faster for smaller radius indicating that the heat flux intensity is directly linked with the strength of the secondary flow. In the plane $z/D_h = 0.25$, we observe a rise of the heat flux starting from the middle of the curved part. It can be explained by the development of the secondary flow close to the sidewalls which drives cold fluid toward the heated convex wall and therefore gives rise to important temperature gradients. In the oblique outflow, Nu increases for both values of z/D_h. In the symmetry plane, this is due to the weakening of the Ekman cells as observed in figure 2 a). In the $z/D_h = 0.25$ plane, the progressive growth of the heat flux is attributable to the impact of cold fluid brought from the duct core towards the heated wall on the external side of the Ekman cells. These cells are concentrated near the duct corner at the beginning of the curvature and progressively move towards the duct core as we move downstream, inducing a progressive displacement of the impact region away from the duct corner. Note that the transverse variations of the heat flux are important since,for instance in the case of $R_c = 4D_h$, at $s/D_h = 6$, Nu is of the order of 10 in the middle plane and 40 for $z/D_h = 0.25$. In figure 2 c), we can note the global large values of the Nusselt number after the curved part. It can be explained by the large impact region of cold fluid compared with the small region of ejection of hot fluid. The diminution of the curvature radius induces a strong increase of the Nusselt number but also a raise of the transverse variation.

5 Conclusion

Large Eddy Simulations are carried out to investigate the influence of the curvature radius, R_c on flow in curved duct. When R_c decreases, we observe

a rise of the intensity of the secondary flow connected to the enhancement of the radial pressure gradient between the two curved walls. The two Ekman cells which develop close to the convex wall are larger in size for small R_c and their centre is thus moved toward the core region. We also observe some modifications on the unsteady vortices of Görtler type which develop on the concave side : their number increases with a reduction of R_c. In this study, we also investigate the influence of R_c on the heat transfer when heating is applied on the convex wall. We observe an increase of the Nusselt number with the reduction of R_c, specially close to the sidewalls where the secondary flow drive cold fluid toward the heated wall: Nu is almost twice as high when the curvature radius is twice as small.

Acknowledgments

Some of the computations were carried out at the IDRIS (Institut du Dévelop pement et des Ressources en Informatique Scientifique, Paris). This work was supported by the CNES (Centre National d'Etudes Spatiales).

References

1. Hunt, I.A., Joubert, P.N. (1979) J. Fluid Mech. 91:633–659
2. Hoffmann, P.H., Muck, K.C., Bradshaw, P. (1985) J. Fluid Mech. 161:371–403
3. Humphrey, J.A.C., Whitelaw, J.H., Yee, G. (1981) J. Fluid Mech. 103:443-463
4. Kim, W.J., Patel, V.C. (1994) J. Fluids Engineering 116:45–52
5. Silva Lopes, A., Piomelli, U., Palma, J.M.L.M. (2003) AIAA 2003-0964
6. Saric, W.S. (1994) Ann. Rev. Fluid Mech. 26:379–409
7. Chang S.M., Humphrey J.A.C., and Modavi A. (1983) PhysicoChemical Hydrodynamics 4(3):243–269
8. Johnson R.W., Launder B.E. (1985) Int. J. Heat and Fluid Flow 6(3):171–180
9. Mayle R.E., Blair M.F., and Kopper F.C. (1979) J.Heat Transfer 101:521–525
10. Hébrard J., Métais O., and Salinas Vasquez M. (2004) Int. J. Heat and Fluid Flow 25:569–580
11. Münch C., Métais O. (2005) C.R. Acad. Sci. Paris. Ser II b, in press
12. Münch C., Métais O. (2005) Mécanique & Industries 6:275–278
13. Salinas Vazquez, M., Metais, O. (2002) J. Fluid Mech. 453:201–238
14. Lesieur, M., Métais, O. (1996) Ann.Rev.Fluid Mech. 28:45–82
15. Kennedy, C.A., Carpenter, M.H. (1997) NASA technical paper Paper 3484
16. Poinsot, T., Lele, S. (1992) J. Comput Phys. 101:104–129
17. Mees, A.J., Nandakumar, K. and Masliyah, J.H. (1996) J. Fluid Mech. 314:227–246
18. Hunt J.R.C., Wray A.A. and Moin P. CTR, Stanford Annual research briefs